ACADEMIC PRESS

Available online at www.sciencedirect.com

SCIENCE DIRECT®

Journal of Sound and Vibration 261 (2003) 153–168

JOURNAL OF SOUND AND VIBRATION

www.elsevier.com/locate/jsvi

Exact solution of the asymmetric Mindlin's plate equations applied to a disk

M. El-Raheb*

1000 Oak Forest Lane, Pasadena, CA 91107, USA

Received 14 May 2001; accepted 29 April 2002

Abstract

An exact solution is presented for the static and dynamic asymmetric response of a disk governed by Mindlin's plate equations forced by a pressure that varies radially as r^m. The static solution agrees with a modal solution adopting the dynamic Mindlin's plate equations in the limit when excitation frequency vanishes. This solution is useful in sizing magnitude and shape of surface asymmetries on a disk from pressure loading with slight eccentricity and circumferential non-uniformity.

1. Introduction

Mindlin's plate equations [1] represent a consistent approximation to the three-dimensional elasto-dynamic equations. One essential feature of these equations is the finite speed of shear waves which lacks in the classical Euler equations. In Cartesian co-ordinates, the equations are separable, yet the solution converges slowly since the dependence along one axis is in terms of hyperbolic functions. For a disk subjected to axisymmetric loading, exact solutions to Mindlin's static and dynamic equations have been treated extensively in the literature. However, the analysis of the static and dynamic problems of a disk loaded asymmetrically is rare.

Karunasena et al. [2] treat the static axisymmetric response of a disk with annular supports adopting Mindlin's plate equations. Irons and Kennedy [3] treat the non-linear axisymmetric frequency response of annular disks. Xiang et al. [4] treat linear axisymmetric frequency response with concentric stiffeners. Soamidas and Ganesan [5] analyze variable thickness polar orthotropic disks. Since 1989, most publications on disks concern magnetic storage devices and focus on rotating thin disks with axisymmetric loading (see Refs. [6–9]). Jia and Lee [10] and Raman and

*Tel.: +1-626-796-5528; fax: +1-626-583-8834.
E-mail address: mertrident@earthlink.net (M. El-Raheb).

0022-460X/03/$ - see front matter
doi:10.1016/S0022-460X(02)00958-6

Mote [11] treat linear asymmetric frequency response of a disk with angular imperfections in properties adopting the classical Euler's equation. Liew and Yang [12,13] solve the three-dimensional free vibration problem of a solid disk and annular plate for symmetric and asymmetric modes by an approximate polynomial-Ritz method.

In what follows, the general static Mindlin's equations are solved exactly for a disk loaded by an asymmetric pressure of the form $p(r,\theta) = p_m r^m \cos n\theta$ acting over a footprint of radius r_p, where (r,θ) are radial and circumferential co-ordinates and n is circumferential wave number. This loading simulates the asymmetry in pressure from eccentricity and circumferential non-uniformity.

In the axisymmetric case, the state vector of dependent variables $\mathbf{S}$ has four components; displacement w, radial rotation ψ_r, and radial shear and moment resultants $Q_r, M_{rr} \Rightarrow \mathbf{S} = \{w, \psi_r, Q_r, M_{rr}\}^{\mathrm{T}}$. The coupled fourth order system of equations yields four primitives and independent constants sufficient to satisfy continuity of $\mathbf{S}$ at an interface of two adjacent disk segments. In the asymmetric case, $\mathbf{S}$ includes two new dependent variables; circumferential rotation ψ_θ and torsional moment resultant $M_{r\theta} \Rightarrow \mathbf{S} = \{w, \psi_r, \psi_\theta, Q_r, M_{rr}, M_{r\theta}\}^{\mathrm{T}}$. The equilibrium equation in ψ_θ raises the order of the system from fourth to sixth allowing for the two additional primitives. To solve the coupled equations in $\{w, \psi_r, \psi_\theta\}^{\mathrm{T}}$, uncoupled equations in each variable are needed. Applying the Helmholtz decomposition to the rotation vector $\mathbf{\Psi} \equiv \{\psi_r, \psi_\theta\}^{\mathrm{T}}$ facilitates the process. $\mathbf{\Psi}$ is expressed as the sum of the gradient of a scalar function and the curl of a vector function, $\mathbf{\Psi} = \boldsymbol{\nabla} g + \boldsymbol{\nabla} \times \mathbf{\Gamma}$, also known as the Helmholtz decomposition. In the dynamic case, g is related to w by the inertia term, while in the static case g is independent of w. The Helmholtz decomposition also applies to the particular solution.

Results from the static solution coincide with results from a different solution in which $\mathbf{S}$ is expanded in terms of the dynamic eigenfunctions. Sections 1 and 2 derive exact solutions of the static and dynamic Mindlin's equations for a disk. Section 3 compares results from the two solutions and presents sensitivity of displacement to disk thickness h, disk radius r_d, and footprint radius r_p.

2. Static analysis

Mindlin's static plate equations may be written in vector form as

$$\frac{D}{2}\left[(1-\nu)\boldsymbol{\nabla}^2\mathbf{\Psi} + (1+\nu)\boldsymbol{\nabla}\Phi\right] - \kappa G h\,(\mathbf{\Psi} + \boldsymbol{\nabla} w) = 0, \tag{1}$$

$$\kappa G h\,(\nabla^2 w + \Phi) + p = 0, \quad \Phi = \boldsymbol{\nabla}\cdot\mathbf{\Psi}, \quad D = \frac{E h^3}{12(1-\nu^2)}, \tag{2}$$

where $\mathbf{\Psi}$ is the vector of rotations, w is the transverse displacement, (ρ, ν) are the density and Poisson ratio, (E, G) are Young's and shear moduli, κ is the shear constant, h is the thickness, p is the applied pressure, ∇^2 is the Laplacian and $\boldsymbol{\nabla}$ is the gradient operator. Taking the divergence of Eq. (1),

$$D\nabla^2\Phi - \kappa G h(\Phi + \nabla^2 w) = 0. \tag{3}$$

Eliminating Φ from Eqs. (2) and (3),

$$\nabla^4 w = \left[\frac{1}{D} - \frac{1}{\kappa G h}\nabla^2\right] p. \tag{4}$$

Eliminating $\nabla^2 w$ from Eqs. (2) and (3) yields

$$D\nabla^2 \Phi = -p. \tag{5}$$

Taking the curl of Eq. (1),

$$\left[\frac{D}{2}(1-v)\nabla^2 - \kappa G h\right](\boldsymbol{\nabla} \times \boldsymbol{\Psi}) = 0, \tag{6}$$

from which it can be inferred that $(\boldsymbol{\nabla} \times \boldsymbol{\Psi})$ is not a function of w while $\boldsymbol{\Psi}$ may be expressed as

$$\boldsymbol{\Psi} = \boldsymbol{\nabla} g + \boldsymbol{\nabla} \times \boldsymbol{\Gamma}, \tag{7}$$

where $\boldsymbol{\Gamma}$ is a vector potential for $\boldsymbol{\Psi}$ independent of w. Substituting Eq. (7) in Eq. (5) using the definition of Φ yields

$$D\nabla^4 g = -p. \tag{8}$$

Substituting Eq. (7) into Eq. (6) using the identity

$$\boldsymbol{\nabla} \times \boldsymbol{\nabla} \times \mathbf{A} = \boldsymbol{\nabla}(\boldsymbol{\nabla} \cdot \mathbf{A}) - \boldsymbol{\nabla}^2 \mathbf{A} \tag{9}$$

produces

$$\left[\frac{D}{2}(1-v)\nabla^2 - \kappa G h\right] \boldsymbol{\nabla}^2 \boldsymbol{\Gamma} = \mathbf{0}. \tag{10}$$

Defining $\boldsymbol{\tau} = \boldsymbol{\nabla}^2 \boldsymbol{\Gamma}$ in Eq. (10) yields

$$\left[\boldsymbol{\nabla}^2 - \frac{12\kappa}{h^2}\right] \boldsymbol{\tau} = \mathbf{0}. \tag{11}$$

Furthermore, since $\boldsymbol{\tau}$ and $\boldsymbol{\Psi}$ are orthogonal, and $\boldsymbol{\Psi}$ is in the plane of the disk, then $\boldsymbol{\tau} = (0,\ 0, \tau_z)$ and $\boldsymbol{\Gamma} = (0, 0, \Gamma_z)$.

For a disk with radius r_d, assume separable expressions for $p(r,\theta)$:

$$p(r,\theta) = p_m(H(r) - H(r - r_p))r^m \cos n\theta, \tag{12}$$

where r_p is footprint radius. For $n \geqslant 2$, a $p(r,\theta)$ uniform along r with $m = 0$ in Eq. (12) is discontinuous along θ at $r = 0$. This sets the constraint that $m \geqslant 1$. Based on the forcing function in Eq. (12), w, ψ_r, ψ_θ take the form

$$w(r,\theta) = w_n(r)\cos n\theta, \quad \psi_r(r,\theta) = \psi_{rn}(r)\cos n\theta, \quad \psi_\theta(r,\theta) = \psi_{\theta n}(r)\sin n\theta. \tag{13}$$

Expanding Eq. (7) in cylindrical co-ordinates,

$$(\psi_{rn}, \psi_{\theta n}) = \left(\frac{\partial}{\partial r}, -\frac{n}{r}\right) g_n + \left(\frac{n}{r}, -\frac{\partial}{\partial r}\right) \Gamma_{zn}. \tag{14}$$

From Eqs. (4), (8) and (10), the homogeneous solutions of w_n, g_n and Γ_{zn} are

$$w_n(r) = \sum_{j=1}^{4} C_{nj} R_{nj}(r), \quad g_n(r) = \sum_{j=1}^{4} \tilde{C}_{nj} R_{nj}(r), \tag{15a, b}$$

$$\Gamma_{zn}(r) = C_{5n} \mathrm{I}_n(k_\tau r) + C_{6n} \mathrm{K}_n(k_\tau r), \quad k_\tau = \sqrt{12\kappa}/h, \tag{15c}$$

where $R_{nj}(r)$ are four primitives of the ∇_n^4 operator and $\mathrm{I}_n, \mathrm{K}_n$ are modified Bessel functions of order n.

In what follows, the subscript n will be dropped from all dependent variables and constants of integration for shortness. Also subscripts h and p will refer to the homogeneous and particular solutions, respectively. Eq. (4) admits primitives in the form

$$R(r) = r^\alpha. \tag{16a}$$

Substituting Eq. (16a) into the homogeneous part of Eq. (4) yields the characteristic equation

$$(\alpha^2 - n^2)((\alpha - 2)^2 - n^2) = 0. \tag{16b}$$

For $n = 0$, Eq. (16b) admits a double root $\alpha = 0$, and a double root $\alpha = 2$ yielding a homogeneous solution:

$$w_h(r) = C_1 r^2 + C_2 r^2 \ln r + C_3 + C_4 \ln r, \quad n = 0. \tag{16c}$$

For $n \geqslant 2$, Eq. (16b) admits the roots

$$\alpha = \pm n, \qquad \alpha = \pm n + 2 \tag{16d}$$

with solution

$$w_h(r) = \sum_{j=1}^{4} C_j r^{\alpha_j}, \quad n \geqslant 2. \tag{17}$$

To determine the contribution of ∇g to $\{\psi_r, \psi_\theta\}$ in Eq. (14), eliminate ψ_θ from the first of Eqs. (1) and (2):

$$\psi_r'' + \frac{3}{r}\psi_r' + \frac{(1-n^2)}{r^2}\psi_r - k_\tau^2 \psi_r = \left(-\frac{2}{r} + \frac{(1+\nu)}{(1-\nu)}\frac{\partial}{\partial r}\right)\left(\nabla^2 w + \frac{p(r)}{\kappa G h}\right). \tag{18}$$

From Eqs. (14) and (15b), the homogeneous solution of ψ_r has the form

$$\psi_{rh}(r) = D_1 r^{n-1} + D_2 r^{-n-1} + D_3 r^{n+1} + D_4 r^{-n+1}. \tag{19}$$

Substituting Eqs. (19) and (17) into Eq. (18) and equating coefficients of the same powers of r to zero yields

$$\begin{aligned}
&- D_1 k_\tau^2 + 4D_3(1+n) = C_1 k_\tau^2 n + 4C_3(1+n)\left(-2 + \frac{1+\nu}{1-\nu} n\right),\\
&- D_2 k_\tau^2 + 4D_4(1-n) = -C_2 k_\tau^2 n - 4C_4(1-n)\left(2 + \frac{1+\nu}{1-\nu} n\right),\\
&- D_3 k_\tau^2 = C_3 k_\tau^2 (n+2), \quad -D_4 k_\tau^2 = C_4 k_\tau^2 (-n+2).
\end{aligned} \tag{20a}$$

Solving for D_i in terms of C_i :

$$D_1 = -nC_1 - \frac{8n(1+n)}{k_\tau^2(1-\nu)}, \quad C_3D_3 = -(n+2)C_3,$$

$$D_2 = nC_2 + \frac{8n(1-n)}{k_\tau^2(1-\nu)}, \quad C_4D_4 = -(-n+2)C_4. \tag{20b}$$

From Eq. (2),

$$\psi_{\theta h} = -\frac{r}{n}\left(\psi'_{rh} + \frac{1}{r}\psi_{rh} + \nabla^2 w_h\right). \tag{21}$$

From Eqs. (14) and (15b), the form of $\psi_{\theta h}$ is

$$\psi_{\theta h}(r) = E_1 r^{n-1} + E_2 r^{-n-1} + E_3 r^{n+1} + E_4 r^{-n+1}. \tag{22}$$

Substituting Eqs. (17), (19) and (22) into Eq. (21) and equating coefficients of equal powers of r yields

$$E_1 = nC_1 + \frac{8n(1+n)}{k_\tau^2(1-\nu)}C_3, \quad E_3 = nC_3,$$

$$E_2 = nC_2 + \frac{8n(1-n)}{k_\tau^2(1-\nu)}C_4, \quad E_4 = nC_4. \tag{23}$$

Adding the contribution of $\boldsymbol{\nabla} \times \boldsymbol{\Gamma}$ in Eq. (14) to Eqs. (19) and (22) determines the complete homogeneous solution of $\{\psi_r, \psi_\theta\}$:

$$\psi_{rh}(r) = D_1 r^{n-1} + D_2 r^{-n-1} + D_3 r^{n+1} + D_4 r^{-n+1} + \frac{n}{r}(C_5 \mathrm{I}_n(k_\tau r) + C_6 \mathrm{K}_n(k_\tau r)),$$

$$\psi_{\theta h}(r) = E_1 r^{n-1} + E_2 r^{-n-1} + E_3 r^{n+1} + E_4 r^{-n+1} - k_\tau(C_5 \mathrm{I}'_n(k_\tau r) + C_6 \mathrm{K}'_n(k_\tau r)). \tag{24}$$

The particular solution w_p of Eq. (4) is determined by the method of variation of parameters. In Eq. (17), assume $C_j = C_j(r)$:

(1) Evaluate w', w'', w''', and w'''' where $()'$ is partial derivative with respect to r.
(2) For the first three derivatives equate terms including $C'_r(r)$ to zero.
(3) Substitute the derivatives in Eq. (4).

This yields four simultaneous equations in C'_j. For $n \geqslant 2$, changing variables to

$$\beta_j = \frac{D}{p_m} C'_j(r) r^{\alpha_j - 3 - m} \tag{25a}$$

eliminates the r dependence from these equations yielding

$$\mathbf{M}\boldsymbol{\beta} = \mathbf{U}, \tag{25b}$$

$$M_{1,j} = 1, \quad M_{2,j} = \alpha_j,$$

$$M_{3,j} = \alpha_j(\alpha_j - 1), \quad M_{4,j} = \alpha_j(\alpha_j - 1)(\alpha_j - 2), \quad (j = 1, 4),$$

$$U_i = \delta_{4i}, \quad \boldsymbol{\beta} = \{\beta_1, \beta_2, \beta_3, \beta_4\}^{\mathrm{T}},$$

where δ_{4i} is the Kronecker delta. Solving for β_j in Eq. (25b), integrating $C_j'(r)$ in Eq. (25a), then substituting C_j back into Eq. (17) produces

$$w_p(r) = \frac{p_m}{D}\sum_{j=1}^{4}\beta_j\left(\frac{r^{4+m}}{4+m-\alpha_j} - \frac{\eta(m^2-n^2)r^{2+m}}{2+m-\alpha_j}\right) = \frac{p_m}{D}\left(\frac{r^{m+4}}{\mu_{mn4}\mu_{mn2}} - \frac{\eta r^{m+2}}{\mu_{mn2}}\right),$$

$$\mu_{mnj} = ((m+j)^2 - n^2), \quad \eta = \frac{h^2}{6(1-\nu)\kappa}. \tag{26}$$

Similarly, the particular solution $g_p(r)$ in Eq. (8) is

$$g_p(r) = -\frac{p_m}{D}\frac{r^{m+4}}{\mu_{mn4}\mu_{mn2}}. \tag{27}$$

Since the Helmholtz decomposition (14) also applies to the particular solution $(\psi_{rp}, \psi_{\theta p})$, then

$$\psi_{rp}(r) = \frac{\partial g_p}{\partial r} = -\frac{p_m}{D}\sum_{j=1}^{4}\beta_j\frac{(m+4)r^{3+m}}{4+m-\alpha_j} = -\frac{p_m}{D}\frac{(m+4)r^{m+3}}{\mu_{mn4}\mu_{mn2}},$$

$$\psi_{\theta p}(r) = -\frac{ng_p}{r} = \frac{p_m}{D}\sum_{j=1}^{4}\beta_j\frac{nr^{3+m}}{4+m-\alpha_j} = \frac{p_m}{D}\frac{nr^{m+3}}{\mu_{mn4}\mu_{mn2}}. \tag{28}$$

When $\mu_{mn2} = 0$, the particular solutions in Eqs. (26) and (28) reduce to

$$w_p(r) = \frac{1}{4n^2}\frac{p_m}{D}\xi_p(r) - \frac{\eta}{2n}\frac{p_m}{D}\left\{r^n \ln r - \frac{r^{m+2}}{(m+2+n)}\right\},$$

$$\xi_p(r) = \left\{\left(\frac{1}{2}\left(1 - \frac{1}{n+1}\right)\ln r - \frac{1}{4}\left(1 - \frac{1}{(n+1)^2}\right)\right)r^{n+2} + \frac{2nr^{m+4}}{(m+2+n)\mu_{mn4}}\right\},$$

$$\psi_r(r) = -\frac{1}{4n^2}\frac{p_m}{D}\frac{\partial\xi_p(r)}{\partial r}, \quad \psi_\theta(r) = \frac{1}{4n}\frac{p_m}{D}\frac{\xi_p(r)}{r}, \tag{29a}$$

and when $\mu_{mn4} = 0$, they reduce to

$$w_p(r) = \frac{p_m}{2Dn\mu_{mn2}}\varsigma_p(r) - \frac{p_m\eta}{D}\frac{r^{m+2}}{\mu_{mn2\theta}},$$

$$\varsigma_p(r) = \left(r^n \ln r - \frac{r^{m+4}}{m+4+n}\right),$$

$$\psi_r(r) = \frac{p_m}{2Dn\mu_{mn2}}\frac{\partial\varsigma_p(r)}{\partial r}, \quad \psi_\theta(r) = \frac{p_m}{2D\mu_{mn2}}\frac{\varsigma_p(r)}{r}. \tag{29b}$$

Eq. (17) and (24) for the homogeneous parts, and Eqs. (26) and (28) or alternatively Eq. (29) for the particular parts, represent the exact solution to the problem.

Constitutive relations for moment and shear resultants are

$$M_{rr} = D\left(\psi_r' + \nu\left(\frac{\psi_r}{r} + \frac{n}{r}\psi_\theta\right)\right), \quad M_{\theta\theta} = D\left(\nu\psi_r' + \frac{\psi_r}{r} + \frac{n}{r}\psi_\theta\right), \tag{30a}$$

$$M_{r\theta} = \frac{D(1-\nu)}{2}\left(-\frac{n}{r}\psi_r + \psi_\theta' - \frac{\psi_\theta}{r}\right), \quad Q_r = \kappa Gh\,(w' + \psi_r), \tag{30b}$$

where

$$w'(r) = \sum_{j=1}^{4} C_j \alpha_j r^{\alpha_j - 1} + w'_p(r), \tag{30c}$$

$$\psi'_r(r) = \sum_{j=1}^{4} D_j(\alpha_j - 1)\, r^{\alpha_j - 2} \; - \frac{n}{r}\left(\frac{1}{r}\,\mathrm{I}_n(k_\tau r) - k_\tau \mathrm{I}'_n(k_\tau r)\right) C_5$$
$$- \frac{n}{r}\left(\frac{1}{r}\,\mathrm{K}_n\,(k_\tau r) - k_\tau \mathrm{K}'_n(k_\tau r)\right) C_6 + \psi'_{rp}(r), \tag{30d}$$

$$\psi'_\theta(r) = \sum_{j=1}^{4} E_j(\alpha_j - 1) r^{\alpha_j - 2} - k_\tau^2\left(C_5 \mathrm{I}''_n(k_\tau r) + C_6 \mathrm{K}''_n(k_\tau r)\right) + \psi'_{\theta p}(r). \tag{30e}$$

$(w'_p, \psi'_{rp}, \psi'_{\theta p})$ are derivatives of the particular solutions in (28). Stresses are related to moment and shear resultants by

$$\sigma_{ij} = \frac{6M_{ij}}{h^2}, \quad ij \equiv rr, \theta\theta, r\theta, \quad \tau_{rz} = \frac{Q_r}{h}. \tag{31}$$

For a disk forced by $p(r, \theta)$ given by Eq. (12), divide the disk into two segments:

(1) In $0 \leqslant r \leqslant r_p$ where p_m is finite, C_6 and two of the C_j multiplying r^{α_j} with $\mathrm{Re}(\alpha_j) < 0$ are dropped for boundedness at $r = 0$. However, the derivatives of these coefficients are needed to obtain the particular solution as in Eqs. (27) and (28) in the method of variation of parameters.
(2) In $r_p \leqslant r \leqslant r_d$, where $p_m = 0$, all six C'_js are kept.

Matching the state vectors $\{Q_r, M_{rr}, M_{r\theta}, w, \psi_r, \psi_\theta\}^{\mathrm{T}}$ of the two parts at the interface $r = r_p$ and satisfying one of the boundary conditions below gives for the

(1) *free edge*:

$$M_{rr}(r_d) \equiv M_{r\theta}(r_d) \equiv Q_r(r_d) = 0. \tag{32a}$$

(2) *simply supported edge*:

$$M_{rr}(r_d) \equiv \psi_\theta(r_d) \equiv w(r_d) = 0. \tag{32b}$$

(3) *clamped edge*:

$$w(r_d) \equiv \psi_r(r_d) \equiv \psi_\theta(r_d) \equiv 0. \tag{32c}$$

This produces nine simultaneous equations in the $C_j^{(1,2)}$ of the two segments.

3. Dynamic analysis

The dynamic Mindlin's plate equations are

$$\frac{D}{2}\left[(1-\nu)\boldsymbol{\nabla}^2\boldsymbol{\Psi}+(1+\nu)\boldsymbol{\nabla}\Phi\right]-\kappa Gh\,(\boldsymbol{\Psi}+\boldsymbol{\nabla}w)=\frac{\rho h^3}{12}\frac{\partial^2\boldsymbol{\Psi}}{\partial t^2}, \tag{33}$$

$$\kappa Gh\,(\nabla^2 w+\Phi)+p=\rho h\frac{\partial^2 w}{\partial t^2},$$

$$\Phi=\boldsymbol{\nabla}\cdot\boldsymbol{\Psi},\quad D=\frac{Eh^3}{12(1-\nu^2)}. \tag{34}$$

Taking the divergence of Eq. (33),

$$D\nabla^2\Phi-\kappa Gh\left(\Phi+\nabla^2 w\right)=\frac{\rho h^3}{12}\frac{\partial^2\Phi}{\partial t^2}. \tag{35}$$

Eliminating Φ from Eqs. (34) and (35) gives

$$\left[\left(\nabla^2-\frac{1}{c_\varepsilon^2}\frac{\partial^2}{\partial t^2}\right)\left(\nabla^2-\frac{1}{c_s^2}\frac{\partial^2}{\partial t^2}\right)+\frac{12}{c_\varepsilon^2 h^2}\frac{\partial^2}{\partial t^2}\right]w=\left[\frac{1}{D}-\frac{1}{\kappa Gh}\left(\nabla^2-\frac{1}{c_\varepsilon^2}\frac{\partial^2}{\partial t^2}\right)\right]p,$$

$$c_\varepsilon^2=\frac{E}{\rho\,(1-\nu^2)},\quad c_s^2=\frac{\kappa G}{\rho}. \tag{36}$$

Eliminating $\nabla^2 w$ from Eqs. (34) and (35) yields

$$\left[D\nabla^2-\frac{\rho h^3}{12}\frac{\partial^2}{\partial t^2}\right]\Phi=\rho h\frac{\partial^2 w}{\partial t^2}-p. \tag{37}$$

Taking the curl of Eq. (33):

$$\left[\frac{D}{2}(1-\nu)\,\nabla^2-\kappa Gh-\frac{\rho h^3}{12}\frac{\partial^2}{\partial t^2}\right](\boldsymbol{\nabla}\times\boldsymbol{\Psi})=\mathbf{0}, \tag{38}$$

from which it can be inferred that $(\boldsymbol{\nabla}\times\boldsymbol{\Psi})$ is not a function of w while $\boldsymbol{\Psi}$ may actually be

$$\boldsymbol{\Psi}=\boldsymbol{\nabla}\,[g(w)]+\boldsymbol{\nabla}\times\boldsymbol{\Gamma}, \tag{39}$$

where $\boldsymbol{\Gamma}$ is a vector potential for $\boldsymbol{\Psi}$ independent of w. Substituting Eq. (39) into Eq. (37) and using the definition of Φ yields

$$\left[D\nabla^2-\frac{\rho h^3}{12}\frac{\partial^2}{\partial t^2}\right]\nabla^2 g=\rho h\frac{\partial^2 w}{\partial t^2}. \tag{40}$$

Substituting Eq. (39) into Eq. (38) using the identity

$$\boldsymbol{\nabla}\times\boldsymbol{\nabla}\times\mathbf{A}=\boldsymbol{\nabla}\,(\boldsymbol{\nabla}\cdot\mathbf{A})-\nabla^2\mathbf{A} \tag{41}$$

produces

$$\left[\frac{D}{2}(1-\nu)\,\nabla^2-\kappa Gh-\rho\frac{h^3}{12}\frac{\partial^2}{\partial t^2}\right]\boldsymbol{\nabla}^2\boldsymbol{\Gamma}=\mathbf{0}. \tag{42}$$

Defining $\boldsymbol{\tau} = \boldsymbol{\nabla}^2\boldsymbol{\Gamma}$ reduces Eq. (42) to

$$\left[\nabla^2 - \frac{12\kappa}{h^2} - \frac{2}{(1-\nu)\,c_\varepsilon^2}\frac{\partial^2}{\partial t^2}\right]\boldsymbol{\tau} = \mathbf{0}. \tag{43}$$

For a solid disk and periodic motions in time with frequency ω, the homogeneous solution of Eq. (36) takes the form

$$w(r,\theta,t) = w(r)\cos n\theta\, \mathrm{e}^{\mathrm{i}\omega t}, \quad w(r) = C_1\mathrm{J}_n(\lambda_1 r) + C_2\mathrm{J}_n(\lambda_2 r), \tag{44a, b}$$

$$\lambda^4 - 2\,\beta_1\lambda^2 + \beta_2 = 0, \quad \beta_1 = \frac{1}{2}\frac{c_\varepsilon^2 + c_s^2}{c_\varepsilon^2\, c_s^2}\;\omega^2, \quad \beta_2 = \frac{\omega^2}{c_\varepsilon^2}\left(\frac{\omega^2}{c_s^2} - \frac{12}{h^2}\right), \tag{44c}$$

where (r,θ) are radial and circumferential co-ordinates, n is circumferential wave number, $\mathrm{i} = \sqrt{-1}$ and J_n is the Bessel function. Since $g(r)$ is a function of w, and from Eq. (8) linear with w, it can be expressed like Eqs. (44a, b) as

$$g_j(r) = C_g\mathrm{J}_n(\lambda_j\, r), \quad \nabla^2 g_j = -\lambda_j^2 g_j, \;\; j = 1,\, 2. \tag{45}$$

Substituting Eq. (45) into Eq. (40) yields

$$-\left[-\lambda_j^2 + \frac{\omega^2}{c_\varepsilon^2}\right]\lambda_j^2 C_{gj} = -\frac{12\omega^2}{h^2\, c_\varepsilon^2}\, C_j, \tag{46}$$

then, using Eq. (36), Eq. (46) simplifies to

$$C_{gj} = \frac{1}{\lambda_j^2}\left(-\lambda_j^2 - \frac{\omega^2}{c_s^2}\right) C_j. \tag{47}$$

Taking the gradient of Eq. (46),

$$\nabla g_j = \left(\frac{\partial}{\partial r}, -\frac{n}{r}\right) C_{gj}\mathrm{J}_n(\lambda_j\, r). \tag{48}$$

Furthermore, since $\boldsymbol{\tau}$ and $\boldsymbol{\Psi}$ are orthogonal and $\boldsymbol{\Psi}$ is in the plane of the disk then $\boldsymbol{\tau} = (0,\, 0, \tau_z)$ and

$$\tau_z = C_\tau\mathrm{J}_n(\lambda_\tau\, r). \tag{49}$$

Substituting Eq. (49) into Eq. (43) produces the dispersion relation

$$k_\tau^2 = \frac{2\omega^2}{(1-\nu)\,c_\varepsilon^2} - \frac{12\kappa}{h^2}. \tag{50}$$

Eq. (50) exhibits a cut-off above

$$\omega_\tau = \sqrt{6\kappa\,(1-\nu)}\,\frac{c_\varepsilon}{h} \;\; = \frac{\sqrt{12}c_s}{h}, \tag{51}$$

which is the same as that in Eq. (44c). Finally, using k_τ in Eq. (50) and since $\boldsymbol{\Gamma}$ and $\boldsymbol{\tau}$ are parallel, then $\boldsymbol{\Gamma} = (0,\, 0, \Gamma_z)$, and

$$\Gamma_z = C_\Gamma\mathrm{J}_n(k_\tau r). \tag{52}$$

Taking the curl of Eq. (52),

$$\nabla \times \Gamma = \left(\frac{n}{r}, -\frac{\partial}{\partial r}\right) C_\Gamma \mathrm{J}_n(k_\tau r). \tag{53}$$

Substituting Eqs. (48) and (53) into Eq. (39) determines the solutions

$$\psi_r(r,\theta,t) = \cos n\theta \, \mathrm{e}^{\mathrm{i}\omega t} \left\{ \sum_{j=1}^{2} C_{gj} \lambda_j \mathrm{J}'_n(\lambda_j r) + \frac{n}{r} C_\Gamma \mathrm{J}_n(k_\tau r) \right\}, \tag{54a}$$

$$\psi_r(r,\theta,t) = \sin n\theta \, \mathrm{e}^{\mathrm{i}\omega t} \left\{ \sum_{j=1}^{2} -\frac{n}{r} C_{gj} \mathrm{J}'_n(\lambda_j r) - \lambda_\tau C_\Gamma \mathrm{J}'_n(k_\tau r) \right\}, \tag{54b}$$

$$w(r,\theta,t) = \cos n\theta \, \mathrm{e}^{\mathrm{i}\omega t} \sum_{i=1}^{2} C_j \mathrm{J}_n(\lambda_j r), \tag{54c}$$

where C_{gi} is related to C_i by Eq. (47). Substituting Eq. (54) into Eq. (30), then in one of the boundary conditions (32), produces the implicit eigenvalue problem

$$\mathbf{B}(r_d)\, \mathbf{C} = \mathbf{0}, \tag{55a}$$

where $\mathbf{B}$ is a 3×3 matrix of the primitives in (ψ_r, ψ_θ, w) and their first derivatives, and

$$\mathbf{C} = \{C_{g_1}, C_{g_2}, C_\Gamma\}^{\mathrm{T}}. \tag{55b}$$

Expanding (ψ_r, ψ_θ, w) in terms of the eigenset $\{\omega_{nj};\ \eta_{rnj}, \eta_{\theta nj}, \varphi_{nj}\}$:

$$\psi_r(r,\theta,t) = \sum_{n=0}^{N} \sum_{j=1}^{M} a_{nj}(t) \eta_{rnj}(r) \cos n\theta, \tag{56a}$$

$$\psi_\theta(r,\theta,t) = \sum_{n=0}^{N} \sum_{j=1}^{M} a_{nj}(t) \eta_{\theta nj}(r) \sin n\theta, \tag{56b}$$

$$w(r,\theta,t) = \sum_{n=0}^{N} \sum_{j=1}^{M} a_{nj}(t) \varphi_{nj}(r) \cos n\theta, \tag{56c}$$

where (M, N) are the number of radial and circumferential modes in the expansion. Substituting Eq. (56) into Eq. (33) and (34) and enforcing the orthogonality of the eigenfunctions yields a set of uncoupled differential equations in the generalized co-ordinates a_{nj} :

$$\ddot{a}_{nj} + \omega_{nj}^2 \, a_{nj} = -\frac{p_{nj}}{N_{nj}} f(t),$$

$$N_{nj} = \rho h \left\langle \varphi_{nj} \middle| r \varphi_{nj} \right\rangle + \frac{\rho h^3}{12} \left[\left\langle \eta_{rnj} \middle| r \eta_{rnj} \right\rangle + \left\langle \eta_{\theta nj} \middle| r \eta_{\theta nj} \right\rangle \right], \tag{57}$$

where $(\dot{\ })$ is the time derivative, δ_{n0} is the Kronecker delta, $f(t)$ is the time dependence of the forcing pulse, and p_{nj} is the generalized force,

$$p_{nj} = p_m \int_0^{r_p} \varphi_{nj}(r) r^m r \, \mathrm{d}r. \tag{58}$$

The solution of Eq. (57) is expressed as a Duhamel integral

$$a_{nj}(t) = -\frac{p_{nj}}{\omega_{nj} N_{nj}} \int_0^t f(\tau) \sin \omega_{nj} (t-\tau) \, d\tau. \tag{59}$$

For periodic motions in time with frequency ω, $f(t) = e^{i\omega t}$ and Eq. (57) reduces to

$$a_{nj} = -\frac{p_{nj}}{N_{nj}(\omega_{nj}^2 - \omega^2)}. \tag{60}$$

In the limit of $\omega = 0$ in Eq. (60), the static solution is recovered.

4. Results

In the parametric analysis to follow, a simply supported disk is assumed to have the following nominal geometric and material properties: $r_d = 3$ in, $r_p = 1$ in, $E = 45 \times 10^6$ psi, $\rho = 3 \times 10^{-4}$ lb s^2/in^4, $v = 0.25$. The disk is forced by the asymmetric pressure given by Eq. (12) with $m = 2$ and $n = 3$. Fig. 1 compares the stress distribution along r from the static solution in Section 1 (Figs. 1(a–d)), to that from the modal solution in Section 2 (Figs. 1(e–h)) with 60 modes in the expansion. Except for the sharper discontinuity in τ_{rz} at $r = r_p$ (compare Figs. 1(d) and (h)), the closeness of results from distinctly different procedures validates the two methods. Note that all variables peak at $r = r_p$, and all stress component decay smoothly for $r > r_p$, as the boundary is approached. This trend suggests that the effect on dependent variable of boundary conditions will diminish with n.

In a $w(r)$ plot, λ_w is the distance between the two intersections of $w(r)$ with the line $w_{max}/2$, where w_{max} is maximum displacement. λ_w, termed the "influence width", is a measure of the spread of w over the disk radius. Fig. 2 shows how magnitude and shape of displacement w varies with n for two thicknesses; $h = 0.2$ in (see Figs. 2(a–d)), and $h = 0.6$ in (see Figs. 2(e–h)). For $n \leqslant 3$, $\lambda_w \simeq r_d/2$ (see Figs. 2(a) and (e)). As n increases, λ_w diminishes as w becomes confined to the vicinity of $r = r_p$. Comparing Figs. 2(a–d) and (e–h) shows that for a fixed n, increasing h reduces λ_w slightly. Fig. 3 depicts the effect of r_p on w. Comparing Figs. 3(a–d) and (a–d) reveals that a smaller footprint r_p reduces λ_w substantially. Plots of $w_{max}(n)/w_{max}(2)$ in Fig. 4(a–c) and $\lambda_w(n)/r_d$ in Figs. 4(d–f) summarize the behavior in Figs. 2(a–d), 2(e–h) and 3(a–d) completely. Fig. 4(a–c) shows that the decay of w_{max} with n is somewhat insensitive to h and r_p.

Finally, Fig. 5 plots $w(r)$ for the axisymmetric case and the loading in Eq. (12) with $n = 0$. In this case $w_{max}(0)$ is two orders of magnitude larger than $w_{max}(2)$. This implies that in order to cause a comparable deformation, asymmetric imperfections in loading must be substantially higher than the axisymmetric imperfections.

5. Conclusion

Exact static and dynamic solutions of Mindlin's equations were derived for a disk loaded by an asymmetric pressure. The Helmholtz vector decomposition is adopted to decouple displacement and the two components of rotation. The method of variation of parameters determines the particular solution. Results of the static solution are identical to those from a modal solution of

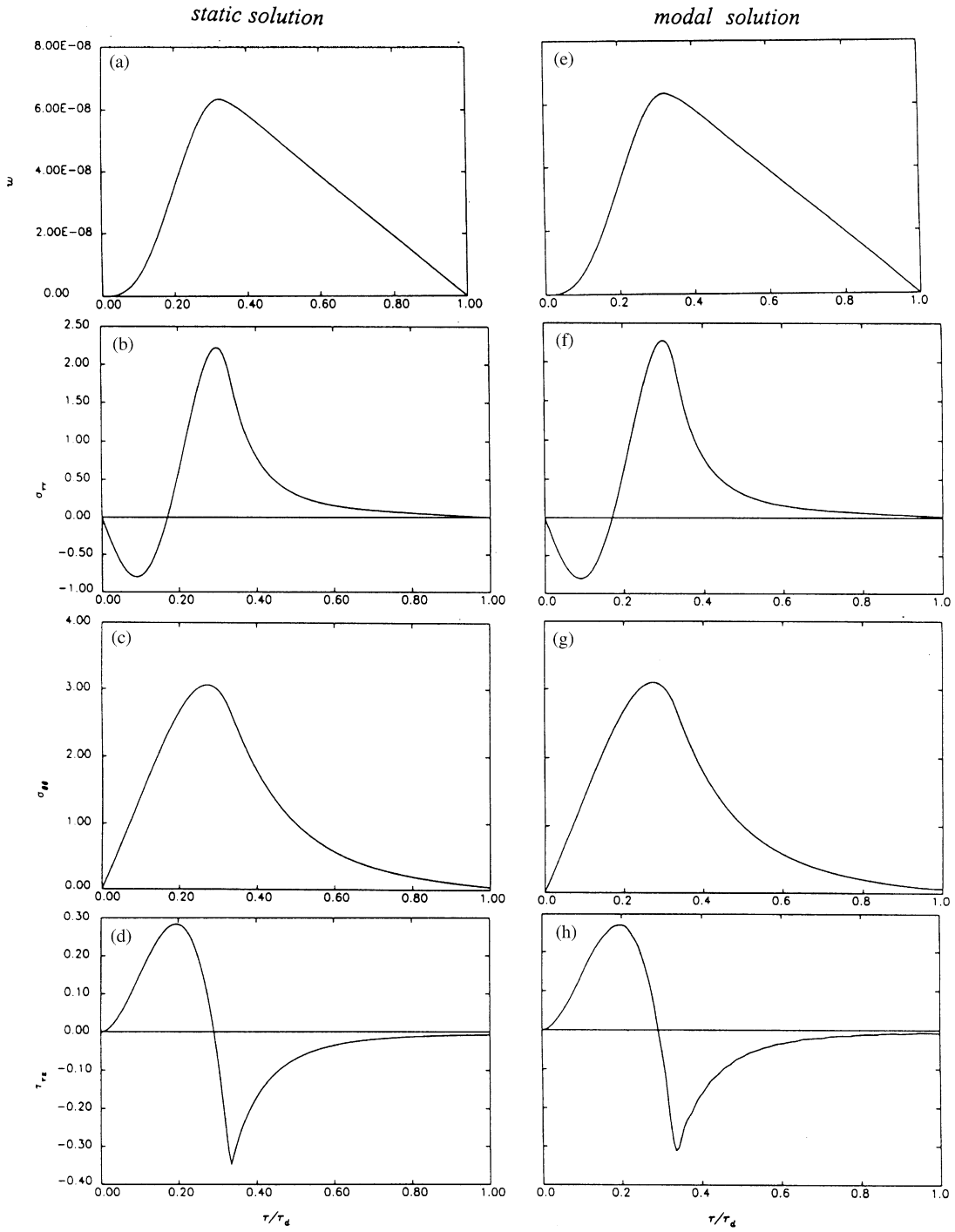

Fig. 1. Comparison of static response from exact and modal solutions ($h = 0.2$ in, $r_p = 1$ in, $n = 3$). Static solution: (a) w, (b) σ_{rr}, (c) $\sigma_{\theta\theta}$, (d) τ_{rz}; Modal solution: (e) w, (f) σ_{rr}, (g) $\sigma_{\theta\theta}$, (h) τ_{rz}.

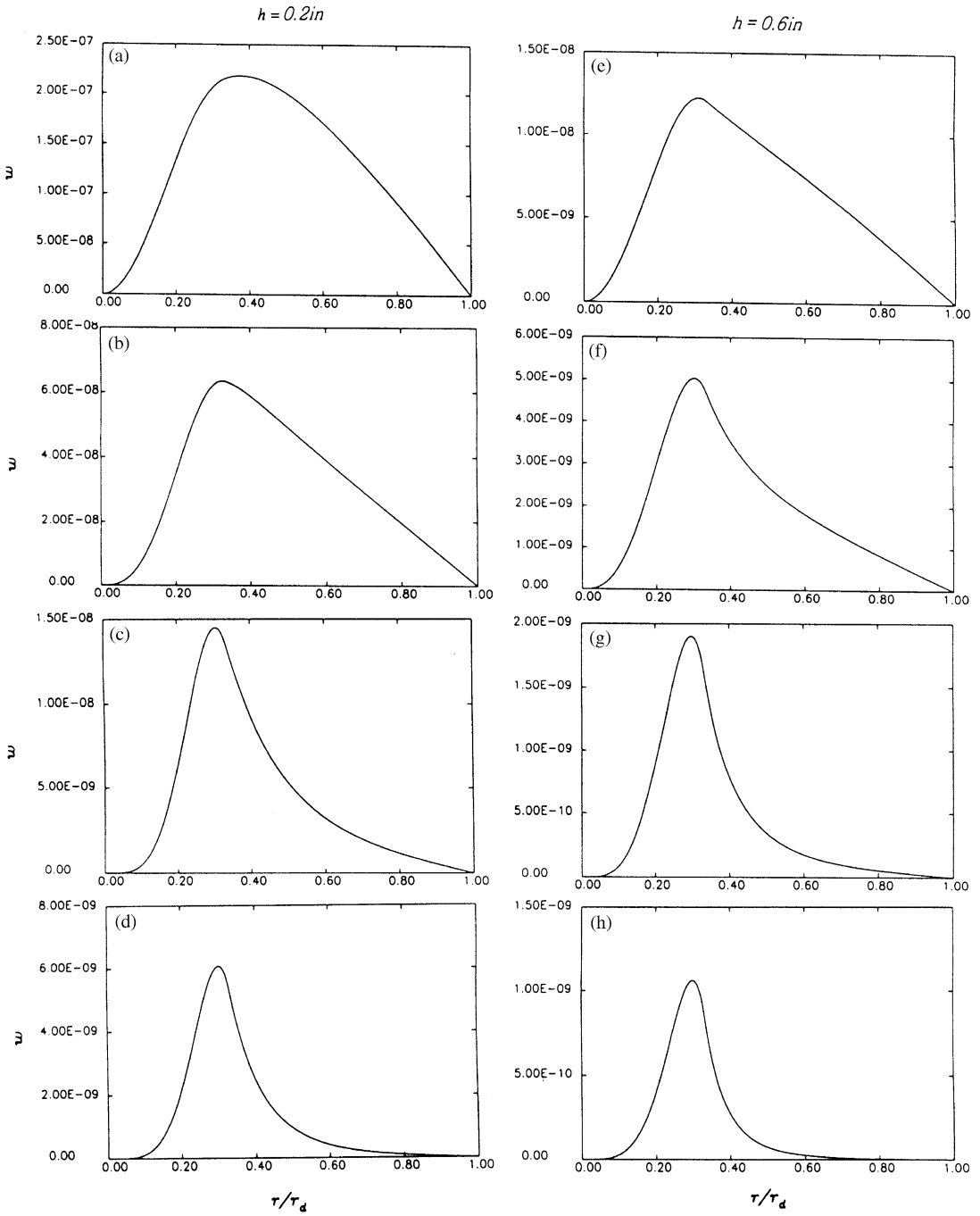

Fig. 2. Effect of h on static w for $r_p = 1$ in; $h = 0.2$ in : (a) $n = 2$, (b) $n = 3$, (c) $n = 5$, (d) $n = 7$; $h = 0.6$ in : (e) $n = 2$, (f) $n = 3$, (g) $n = 5$, (h) $n = 7$.

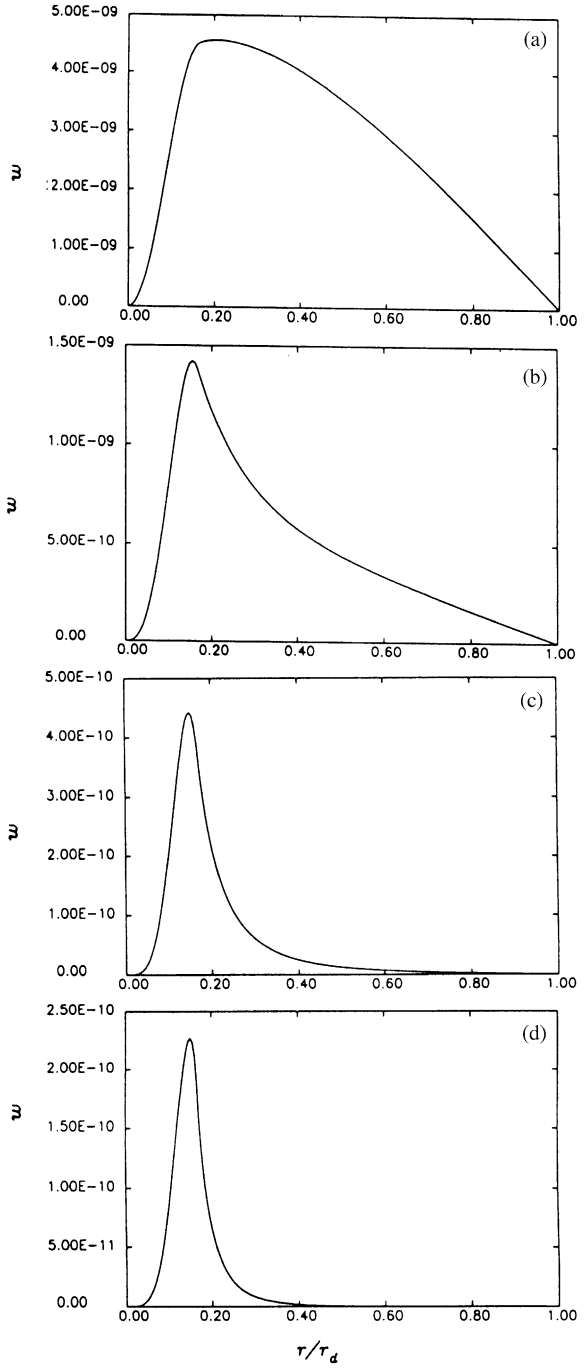

Fig. 3. Static w for $r_p = 0.5$ in, $h = 0.2$ in : (a) $n = 2$, (b) $n = 3$, (c) $n = 5$, (d) $n = 7$.

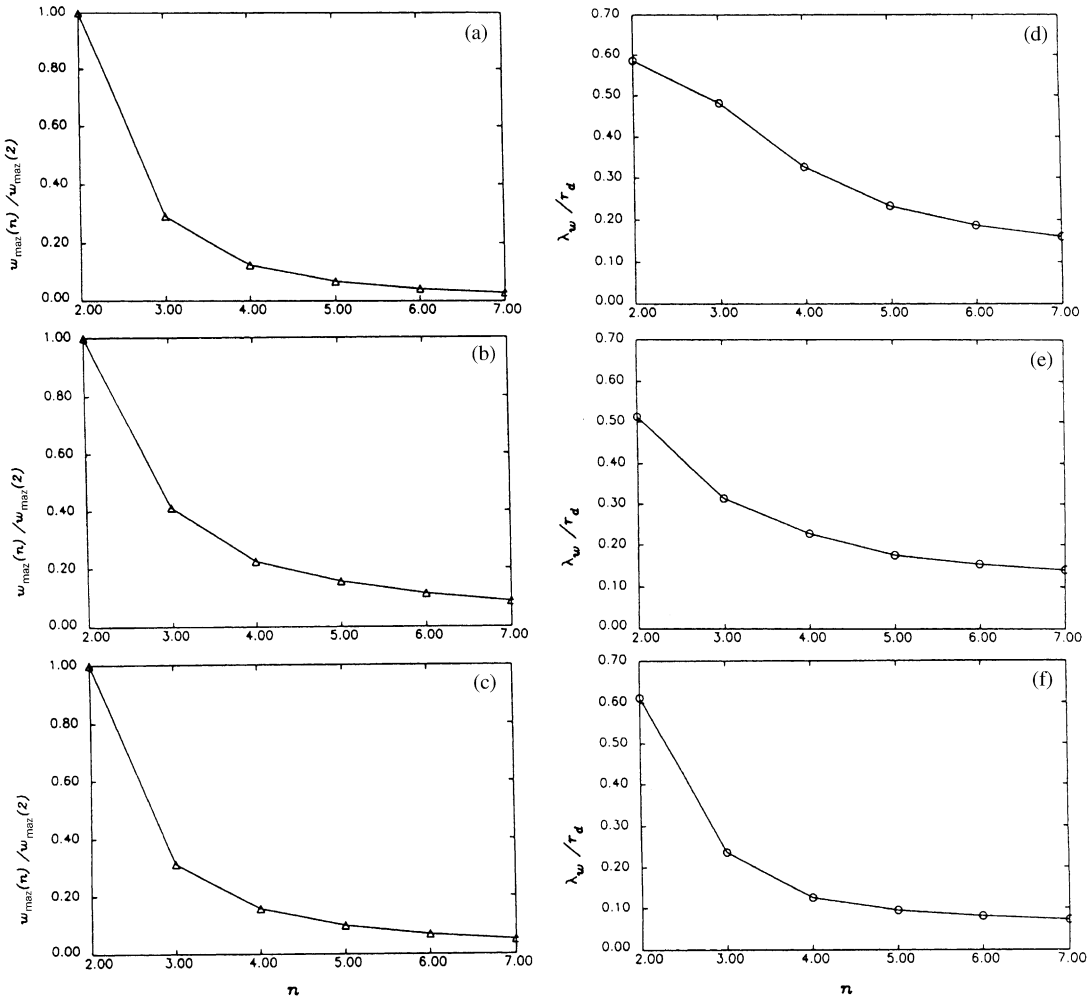

Fig. 4. Variation of $w_{max}(n)/w_{max}(2)$ with n: (a) $h = 0.2$ in, $r_p = 1$ in; (b) $h = 0.6$ in, $r_p = 1$ in; (c) $h = 0.2$ in, $r_p = 0.5$ in; and variation of λ_w/r_d with n: (d) $h = 0.2$ in, $r_p = 1$ in; (e) $h = 0.6$ in, $r_p = 1$ in; (f) $h = 0.2$ in, $r_p = 0.5$ in.

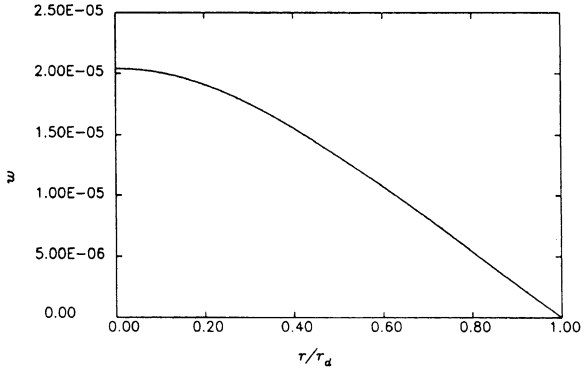

Fig. 5. $w(r)$ for axisymmetric loading ($n = 0$).

the frequency response when frequency vanishes. A parameter λ_w, termed influence width, measures the spread of w over the disk radius. w_{max} and λ_w diminish with n, since w is confined near the perimeter of the footprint. A thicker disk and a narrower footprint reduce λ_w, however, r_p has a stronger effect. Axisymmetric displacement w_0 of the disk forced by the same pressure intensity and radial distribution as that in the asymmetric case is two orders of magnitude larger than w_n for $n = 2$ suggesting that the incremental displacement from asymmetric loading imperfection is negligible.

References

[1] R.D. Mindlin, Influence of rotary inertia and shear deformation on flexural motions of isotropic elastic disks, American Society of Mechanical Engineers Journal of Applied Mechanics 73 (1951) 31–38.
[2] W. Karunasena, C.M. Wang, S. Kitipornchai, Y. Xiang, Exact solutions for axisymmetric bending of continuous annular plates, Computers and Structures 63 (1997) 455–464.
[3] J. Irons, W. Kennedy, Nonlinear vibration of centrally clamped thin disks, International Journal of Nonlinear Mechanics 24 (1989) 345–352.
[4] Y. Xiang, K.M. Liew, S. Kitipornchai, Vibration of circular and annular Mindlin plates with internal ring stiffners, Journal of the Acoustical Society of America 100 (1996) 3696–3705.
[5] V. Soamidas, N. Ganesan, Vibration analysis of thick, polar orthotropic, variable thickness annular disks, Journal of Sound and Vibration 147 (1991) 39–56.
[6] M. Mignolet, C. Eick, M. Harish, Free vibration of flexible rotating disks, Journal of Sound and Vibration 196 (1996) 537–577.
[7] A. Cote, N. Atalla, J. Nicolas, Effects of shear deformation and rotary inertia on the free vibration of a rotating annular plate, Journal of Vibration and Acoustics: Transactions of American Society of Mechanical Engineers 119 (1997) 641–643.
[8] R. Parker, P. Sathe, Exact solutions for the free and forced vibration of a rotating disk–spindle system, Journal of Sound and Vibration 223 (1999) 445–465.
[9] J. Tiang, S. Hutton, Self excited vibration in flexible rotating disks subjected to various transverse interactive forces: a general approach, Journal of Applied Mechanics Transactions of American Society of Mechanical Engineers 66 (1999) 800–805.
[10] H. Jia, C. Lee, On the vibration of imperfect circular disks, Korean Society of Mechanical Engineers International Journal 12 (1998) 223–232.
[11] A. Raman, C. Mote, Effects of imperfection on the nonlinear oscillations of circular plates spinning near critical speed, International Journal of Nonlinear Mechanics 36 (2001) 261–289.
[12] K.M. Liew, B. Yang, Three-dimensional elasticity solutions for free vibrations of circular plates: a polynomials-Ritz analysis, Computer Methods in Applied Mechanics and Engineering 175 (1999) 189–210.
[13] K.M. Liew, B. Yang, Elasticity solutions for free vibrations of annular plates from three-dimensional analysis, International Journal of Solids and Structures 37 (2000) 7689–7702.